

Opo-time of flight system for multiphoton ionization and dissociation studies

E. Mejia-Ospino^{a,b}, I. Alvarez^a, and C. Cisneros^a

^aCentro de Ciencias Físicas, Universidad Nacional Autónoma de México, Cuernavaca, Mor. México,

^bLaboratorio de Espectroscopia Atómico y Molecular, Universidad Industrial de Santander, Bucaramanga, Colombia

Recibido el 27 de mayo de 2003; aceptado el 4 de septiembre de 2003

The design and operation of a time-of-flight mass analyzer for study of ionization and dissociation of atoms and molecules produced by interaction with pulsed laser generated by an OPO are described. This apparatus allows the investigation of atomic and molecular excited states no accessible by single-photon absorption. The description of the main parts as well as the associated instrumentation, and results of multiphoton absorption of xenon and acetone are presented.

Keywords: Multiphoton; TOF; REMPI.

En este trabajo se describe el diseño y la operación de un analizador de masas tipo tiempo de vuelo, para el estudio de la ionización y disociación de átomos y moléculas inducidos por la interacción con la radiación láser proveniente de un sistema OPO. Este aparato permite la investigación de estados excitados de átomos o moléculas no accesibles por la absorción de un solo fotón. Presentamos la descripción de los elementos principales del sistema, así como los resultados de la absorción multifotónica del xenón y la molécula de acetona.

Descriptores: Multifotoionización; multifotodiscociación; espectrometría de tiempo de vuelo.

PACS: 32.10Bi; 32.80Fb; 33.15Ta

1. Introduction

Time of flight mass spectrometry (TOF-MS), an early arrival in the mass spectrometry family, was prominent in the field during the 1960's but soon was displaced by magnetic and quadrupole instruments with higher sensitivity and mass resolving power. The most significant reason for the failure of TOF to mature, was the lack of technologies to produce ions and to facilitate the recording and processing of the mass spectrum in the microsecond time frame. These technologies are now emerging along with methods for the ionization of massive biological molecules and also for fast mixture separation. TOF is highly advantageous in these cases and is therefore reappearing as a prominent mass analyzer.

The study multiphoton processes have been possible by the introduction of high power lasers. The term multiphoton ionization is generally used to define a process where two, or more than one photon are absorbed by a system (atomic or molecular) to reach either the first ionization potential or an excited state over the ionization potential. The multiphoton ionization is possible with uv and vis photons while normal photoionization (single-photon) requires vuv.

The efficiency of the multiphoton ionization is increased when exists an excited state resonant which can be reached with an integer number of incident photons. This process is named Resonance Enhancement Multiphoton Ionization, REMPI, in this case, multiphoton process occurs in two steps: excitation to intermediate states and absorption of more photons to reach the ionization potential. If n is the number of photons required to fit exactly the resonant step and m to the subsequent number of photons required to ionize the atom or molecule, the notation $(n + m)$ is the notation to describe the

REMPI process. If there is not a resonant state involved, the Multiphoton Ionization for the process is called MPI (Fig. 1)

Many molecules are transparent to the wavelength used in REMPI (uv and vis), this means that $n > 1$. The probability to reach intermediate resonant step is very low, however, the resonant step can be characterized easily and n calculated. This is the basis to interpretation of the multiphoton spectra [1,2]. The case of multiphoton dissociation is similar, it

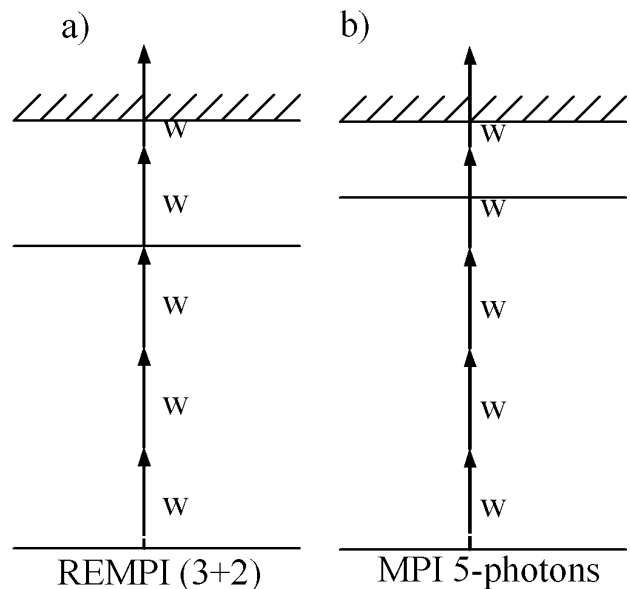


FIGURE 1. a) Resonance enhancement of multiphoton ionization; b) Multiphoton ionization no resonant.

take place when more than one photon is needed to dissociate a molecule.

The purpose of the present work is to present the design, set up and operation of a system to study multiphoton process in atomic and molecular systems, the calibration with xenon and its isotopes multiphoton ionized at 499.050 nm and to illustrate the capabilities of the apparatus. In section 2 is reported an outline of the general setup whereas the detailed description of its parts is located in the next sections. As an example is shown the results for the resonant multiphoton ionization and dissociation of the acetone via the 3s-Rydberg state at 585.000 nm.

2. Experimental system

Figure 2 shows the schematic diagram of the experimental apparatus. The experimental set up consists, basically, of an Nd:YAG-OPO laser, introduction sample system, time of flight spectrometer, the electron energy analyzer [3] and the vacuum system.

The multiphoton absorption with the ionization and dissociation takes place into the time of flight spectrometer. The cations are accelerated at around 4 keV by three parallel electrodes with Wiley-McLaren [12] condition so that the cations were spatially focused through 1m free-field region. In order to optimize the focusing properties of the system the ion trajectories were simulated using the SIMION program.

The TOF system was pumped by two turbo molecular pump with a pumping rate of 450 l/s (Leybold, Turbovac 450) both backed up by an oil-free scroll pump (Alcatel, Drytel 31). The first turbo molecular pump is located below the interaction region while the second is in the detection region. The base pressure in the TOF spectrometer is about 4×10^{-8} Torr. When the pulsed nozzle is operated the pres-

sure decrease until 8×10^{-5} Torr. A pulsed valve of 0.8 mm and a skimmer of 1 mm of diameter were used to introduce the gaseous sample in the interaction region to be exposed to the intense laser pulse field ($10^{10} - 10^{12} \text{ w cm}^{-2}$). Three different ways of operation are available, two in the internal mode (single pulse or cycle of pulses) and one in the external mode (single pulse). Additionally it has two modes to control the time and to maintain the valve open or closed, the first runs from 5 μs to 999 minutes and the second from 0.1 ms to 999.9 minutes. The laser is aligned in such a way that the atomic or molecular beam, the accelerating field and laser beam are perpendicular to each other and intersect at the center between the electrodes.

The Optical Parametric Oscillator, OPO (Spectra Physics, MOPO-730) pumped by the third-harmonic of the Nd:YAG laser (Spectra Physics, Quanta-Ray PRO-210), provides pulses of high intensity and tunable between 450 to 680 nm. The laser beam was focused in the interaction region by a quartz lens ($f=150$ mm), and the direction of the laser polarization was set parallel to the direction axis of the mass spectrometer. With the intensity of the laser in the range of 10^9 to 10^{12} Wcm^{-2} the spot size at the focal length of the lens is of order of microns. The energy per pulse was measured at the exit of the TOF with a Moletron energy meter (Moletron J25).

The energy distribution of the electron produced by the ionization process is measured by a double focusing electrostatic analyzer of spherical sector of 160° , located at 4.5 cm from the mesh electrodes whereas the heavy ions formed in the interaction region are detected at the far end of the tube by a channel electron multiplier or a channel plate. The signal from the detector is amplified by fast electronics and send to a multichannel scaler (EG&G ORTEC, turbo -MCS) where is stored by the arrival time to the detectors.

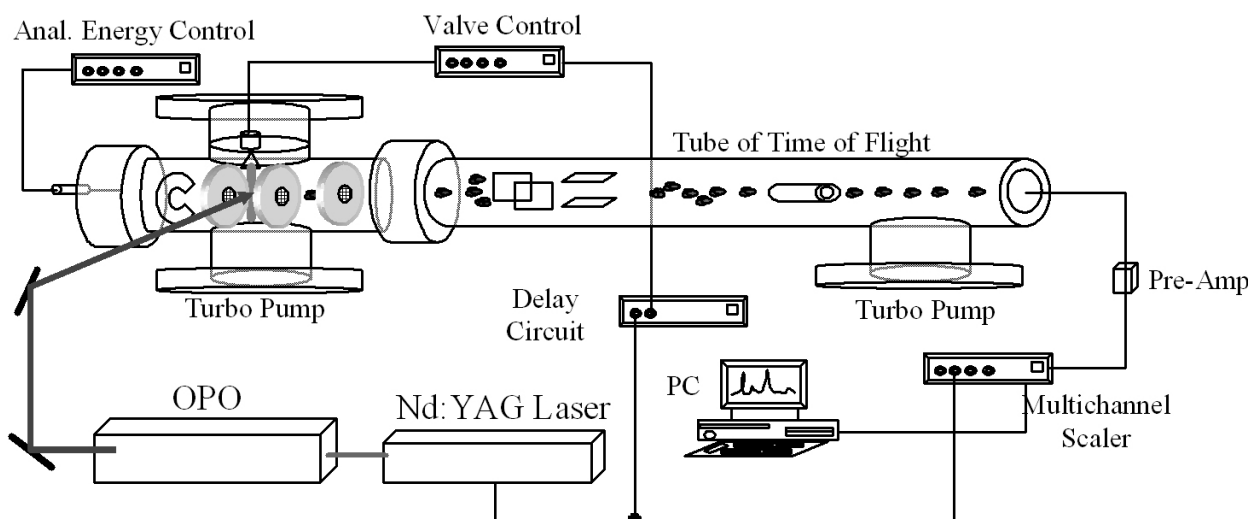


FIGURE 2. Experimental set up of the time-of-flight mass analyzer for a laser induced multiphoton process.

3. Laser system

3.1. Nd:YAG laser

The properties of neodymium-doped yttrium aluminum garnet (Nd:YAG) are the most widely studied and best understood of all solid-state laser media. There are several references that explain the operation principles of this laser [5]. Briefly, the active medium is triply ionized neodymium, which is optically pumped by a flash lamp whose output matches the main absorption bands in the red and near infrared. Excited electrons quickly drop to the $^4F_{3/2}$ level, the upper level of the lasing transition, where they remain for a relatively long time (about 230 μ s). The most probable transition corresponds to the $^4I_{11/2}$ level, emitting a photon at 1064 nm. The temporal width of laser pulse, in this condition, is relatively long. When a Q-switch is added to the resonator to shorten the pulse, the output peak power is raised dramatically [4]. The resultant pulse width is <10 ns, and the peak optical power is ten of megawatts. This high peak power permits frequency conversion in nonlinear crystals like potassium dideuterium phosphate (KD*P). In the simplest case, the 1064 nm Nd:YAG fundamental interacts with the crystal to produce a secondary wave with half the fundamental wavelength. The resultant 532 nm wave can be doubled again, by passing through a second crystal, to yield a 266 nm wave. The 532 nm wave can also be mixed in KD*P crystal with residual 1064 nm to produce a 355 nm pulse. Photons of 355 nm are used to pump the optical parametric oscillator [6].

3.2. Optical parametric oscillator

The principle of operation for the Optical Parametric Oscillator (OPO) is quite different from a conventional laser system. The laser derives its gain from the spontaneous and stimulated emission generated by atomic transitions. These atomic transitions have inherent linewidths that define the maximum tuning range of the laser. For example, a dye laser tunes over 20 nm per dye while Ti:Sapphire lasers can be tuned over 200 nm. In contrast, at 355 nm, BBO based OPO can be tuned continuously from 410 to 4000 nm.

The gain of an OPO arises from a nonlinear interaction between an intense optical wave and a crystal having a large nonlinear polarizability coefficient [5]. OPO operation can be easily understood as the inverse of the process used to generate odd harmonic of the Nd:YAG. An OPO works in the reverse fashion, the energy contained in a pump photon at frequency ω_p is transferred to two other photons, ω_s (the signal wave) and ω_i (the idler wave) in such a way as to satisfy the energy conversion law: $\omega_p = \omega_s + \omega_i$, or in terms of wavelengths: $1/\lambda_p = 1/\lambda_s + 1/\lambda_i$.

The OPO (Spectra Physics, MOPO-730) uses a BBO crystal (Beta Barium Borate) placed in an appropriate resonant cavity where the signal and/or idler wavelength can be obtained. In OPOs, the gain can be large enough that no signal input wave is necessary. The signal will grow from the quantum noise in the crystal. The signal and idler beam exhibit strong coherence, are highly monochromatic, and have a spectrum consisting of one or more longitudinal modes. In the MOPO system, the pump wavelength λ_p is always 355 nm [6].

The MOPO-730 is a coupled dual oscillator system, a high energy Power Oscillator and the Master Oscillator. This system enables the coupled oscillator system to produce narrow bandwidth, high energy and tunable coherent radiation. The MOPO-730 is a pulsed Optical Parametric Oscillator, which use phase, matched Beta Barium Borate (BBO) as nonlinear gain medium. BBO is a negative uniaxial crystal with intrinsic birefringence properties that are used to achieve critical phase matching. Tuning the MOPO output is, therefore, accomplished by rotating the BBO crystal with respect to the optical axis of the resonator [6].

4. Introduction of the sample: supersonic beams

To study the quantum states of molecules at very high resolution two difficulties arise. The first of these is to obtain a sample of the molecule at a temperature, which is low enough, both to prevent thermal dissociation and to produce only as many rotational, and vibrational lines as can be separately assigned in the spectrum. The second difficulty lies in finding a medium that will support the molecular system at this low temperature without introducing undesirable changes and complications in the spectra. An appropriate spectroscopic sample would be an ensemble of molecules, all in a particular and well-defined quantum state, traveling in free space with a narrow velocity distribution, and at a sufficiently low density so that interactions between molecules are negligible.

Two types of molecular (or atomic) beam are known: the effusive and supersonic molecular beam. The earliest and the most familiar molecular beam $D \ll \lambda_0$, where D is the diameter of the aperture and λ_0 is the mean free path of the gas at pressure P_0 , inside the reservoir. In an effusive source, the flow from the aperture is free since there are substantially no collisions between gas molecules downstream of the orifice and the velocity distribution in the beam corresponds to the Maxwell-Boltzmann velocity distribution, characteristic of the reservoir temperature. More important from the point of view of the spectroscopist is the fact that the distribution of internal molecular states is identical with that in the reservoir (Fig. 3a).

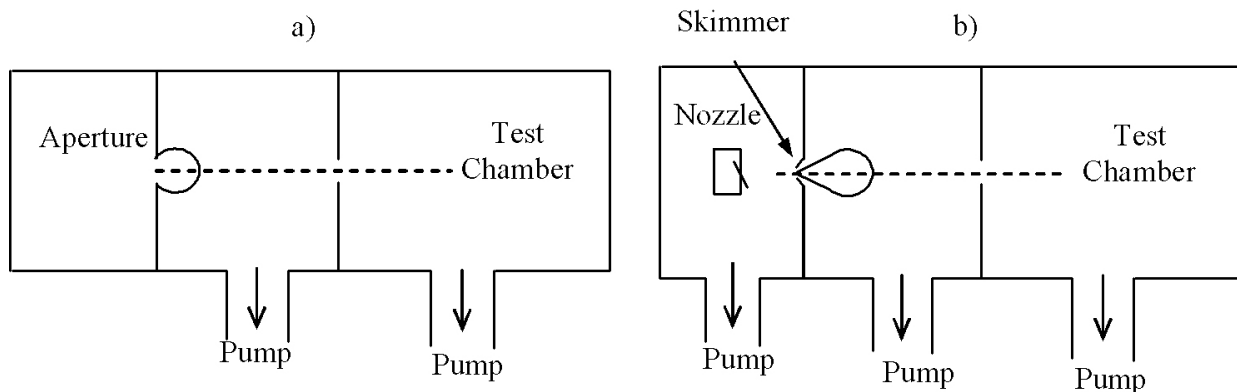


FIGURE 3. Effusive system (a); Supersonic beam system (b).

In 1951, Kantrowitz and Grey [7,8] proposed the supersonic jet as a molecular beam source. Although their motivation seemed to have been primarily an improvement to the beam intensity, they were fully aware that their suggested source would also produce a cooling of the translational and internal degrees of freedom of the molecules in the beam. In the supersonic jet, the reservoir pressure or the aperture size are increased to the point where $D \gg \lambda_0$. There will be many collisions as the gas flows through the orifice and downstream of the aperture, and such a flow regime is called hydrodynamic. The hydrodynamic expansion converts the enthalpy associated with random atomic motion into directed mass flow; this process therefore causes the mass flow velocity, u , to increase. The conversion of random motion to directed mass flow causes the temperature to decrease, and since the classical speed of sound, a , is defined as $(\gamma kT/m)^{1/2}$, where γ is the heat capacity ratio, C_p/C_v , T is temperature and k is the Boltzmann constant. The speed of sound decreases when the Mach number, $M = u/a$, increase. In ideal expansion the number Mach is unity at the most constricted point of the nozzle, and with additional expansion $M > 1$, the flow becomes supersonic. Kantrowitz and Grey emphasized the use of a skimmer to maintain adequately low downstream pressures (Fig. 3b).

Dashed curve in Fig. 4 shows the behavior of an effusive beam where the velocity distribution is given by the Maxwell-Boltzmann velocity distribution. This distribution has a peak at $v = (3kT/m)^{1/2}$ and a standard deviation in velocity $= (0.47kT/m)^{1/2}$. Solid curve in Fig. 5 corresponds to a gas that is expanded through a supersonic nozzle. It has a

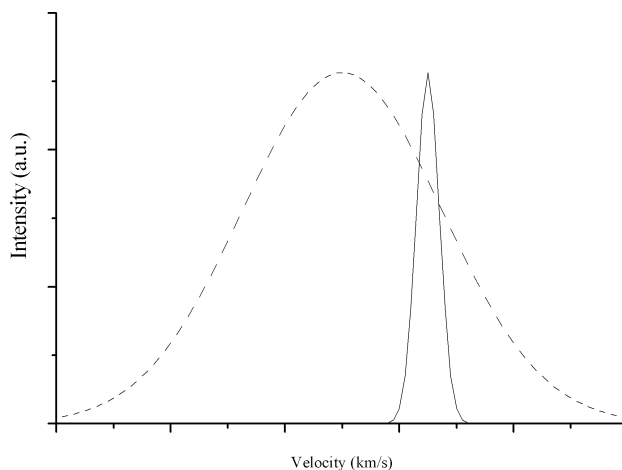


FIGURE 4. Velocity distribution in the effusive regime (—) and hydrodynamic regime (---).

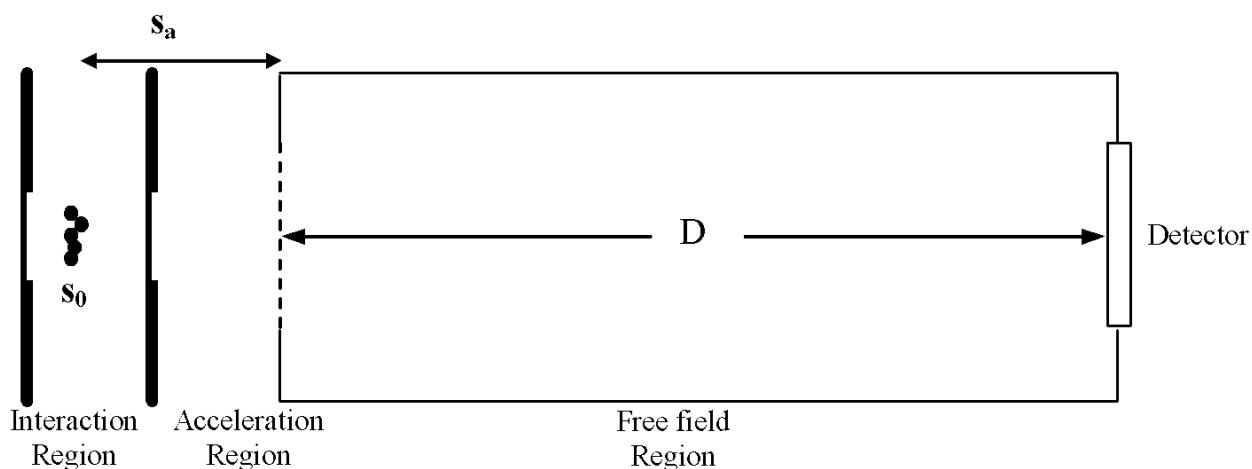


FIGURE 5. Schematic diagram of the time of flight spectrometer.

velocity distribution in the direction of mass flow. Because of the increase in flow velocity, the peak of the distribution is shifted to higher velocity, and because the gas has been cooled, the distribution narrows. The translational temperature is determined by the width of the velocity and not by the position of the peak [9].

A supersonic expansion of molecules in an inert, monoatomic carrier gas, can be in principle fulfill the requirements of an ideal spectroscopy sample. In the case of a supersonic expansion, the translational temperature of the gas carrier can fall to an extremely low value (less 0.03 K in some cases). Polyatomic molecules seeded into this expanding gas interact with the low temperature bath provided by the monoatomic carrier via two-body collisions, causing translational and rotational cooling of the molecules.

Atomic gases are preferable to the molecular gases in obtaining the lowest temperature because they do not store energy in rotational and vibrational degrees of freedom. Hence, for a given expansion ratio they will achieve a lower temperature. A free jet of pure helium has been shown capable of cooling to 0.03 K through expansion into vacuum from room temperature and about 100 atm, and pure argon can be cooled to 2 K or so [8]. In the present design the supersonic jet system is used and it consists of two elements: an electromagnetic pulsed valve (nozzle) that permits the escape of the sample to the interaction region through of an orifice about 0.8 mm of diameter. The valve consists of a piston coupled at a spring that is contracted or expanded magnetically with a fix frequency. The aperture is closed with a Teflon stopper (poppet) when the spring is expanded. The second part is a conic collimator (skimmer) that permits select and directed the high-density zone of the beam to the interaction region.

5. Time of flight mass spectrometer

Mass spectrometry is primarily concerned with measuring the mass-to-charge ratio (m/z) and abundance of ions moving at high speed in a vacuum. Nearly a century of research in mass spectrometry has established that it is one of the most powerful probes of the structure and composition of matter. Since J.J. Thomson's invention of the magnetic detection mass spectrometer, in the first decade of this century, many designs and descriptions of devices for determining the relative yields of ions as a function of m/z have been published. Currently there is increasing interest in mass spectrometry and this results from the advent of new ionization methods and the wider use of compact mass spectrometers. New ionization methods allow the characterization of a diverse range of polar, ionic or high molecular-weight compounds which previously were not amenable to mass spectrometric analysis. Compact mass spectrometers are increasingly used as detectors for chromatographic separations because of their capacity to identify and quantify compounds in complex mixtures, simultaneously.

TOF mass spectrometers differ fundamentally from scanning instruments in the fact that they involve temporally dis-

crete ion formation and mass dispersion in the time domain, rather than along a spatial axis.

The essential principle of TOF-MS is that a population of ions moving in the same direction and having a distribution of masses but a (almost) constant kinetic energy, will have a corresponding distribution of velocities inversely proportional to the square root of m/z . Consider a situation in which ions, under the influence of an external electric field, begins their acceleration from rest at the same time and from the same spatial plane normal to the acceleration vector, their arrival times at a target plane (parallel to the plane of origin) will be distributed according to the square root of m/z . A scheme of the TOF-MS is shown in Fig. 5. It consists, basically, of three regions; interaction or ionization region, acceleration region and free field region. Two electrode-meshes of stainless steel, separated about 1 cm, delimit the first region. Both electrode-meshes have an aperture of 1 cm of diameter; a reticular grid of 95% of transmittance covers these orifices. Each plate is held at different potential to generate a constant electric field that is able to separate positive ions and electrons in opposite direction. The positive ions escape through the grid at the second region (acceleration region) delimited by third plate with ground potential, this plate has a orifice covered by a reticular grid of 99% of transmittance; the second a third electrodes are separated 3 cm. The electrons are directed to a double focusing energy analyzer.

The field free region has 1 m of length and begins in the third plate and ends in a detector. The detector is a channeltron multiplier. In this region occurs most of the separation of the ions and there is neither electric nor magnetic field. The system allows changing either the horizontal or the vertical direction of the ions using a set of steering plates of 2 cm². There are also Einzel lens to focus the ion beams.

In the case of subrelativistic velocities (as occurs in the keV energy regime) a good description of the TOF-MS experiment requires no more than Newtonian physics as shown by the equations that follow [10-12]:

Force and acceleration:

$$a = \frac{Eq}{m}. \quad (1)$$

Velocity and time:

$$u = u_0 + \left(\frac{Eq}{m}\right)t, \quad (2)$$

$$t_a = \frac{u - u_0}{E} \left(\frac{m}{q}\right). \quad (3)$$

Position:

$$s = s_0 + u_0 t + \frac{1}{2} \left(\frac{Eq}{m}\right)t^2. \quad (4)$$

Drift velocity and accelerating voltage:

$$qEs_a = \frac{1}{2}mu_D^2, \quad (5)$$

$$u_D = \sqrt{\frac{2qEs_a}{m}}. \quad (6)$$

Drift time:

$$t_D = \frac{D}{\sqrt{\frac{2qEs_a}{m}}}. \tag{7}$$

Time Of Flight:

$$TOF = t_0 + t_a + t_D + t_d. \tag{8}$$

Where m and q are the mass and charge of the ion, s_0 is the initial position of the ions, s_a is the distance from s_0 to the drift region, u_0 and u_D are the initial and drift velocity, E is the electric-field strength, t_0 is time after $t = 0$ that ion begins to accelerate, t_a is time that the ion is accelerating from u_0 to u_D , t_D is time that ion drifts at constant velocity, D is drift distance and t_d is response time of detection system.

6. Electrostatic energy analyzer

To measure the energy distribution of the electrons produced by the interaction between photons and atoms or molecules there is a double focusing electrostatic energy analyzer of spherical sector of 160° (COMSTOCK AC-900B). Applying appropriate voltage at the plates of the spherical sector is generated a spherical an electric field function of $1/r^2$; the electrons with a given energy range will be transmitted between the inner and outer spherical sector surfaces of the analyzer and refocused upon the exit aperture.

The analyzer consists basically of two concentric spherical sector surfaces, an inner convex and an outer concave of ratios R_1 and R_2 respectively. The two surfaces, machined from oxygen free copper and then polished, are accurately held in position on a common center, and insulated from each other by a sapphire ball located in hole drilled in side a the copper side and end plates (Fig. 6).

The resolution of the spherical sector analyzer is given by

$$\Delta E = \frac{w}{R(1 - \cos \phi) + L \sin \phi} (TE), \tag{9}$$

where TE is the energy of transmission, w diameter of the entrance and exit apertures, R is the main sphere radius, ϕ is

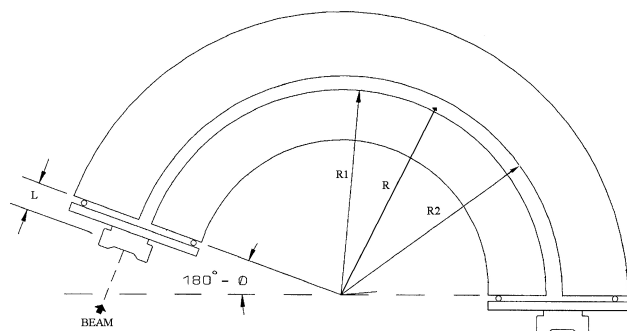


FIGURE 6. Electrostatic energy analyzer of spherical sector.

the angle subtended by analyzer sector, L is the distance from the exit of the sector field to the center of the exit aperture [14].

The energy of the transmitted electrons is determined by

$$TE = \frac{\Delta V}{\frac{R_2}{R_1} - \frac{R_1}{R_2}}, \tag{10}$$

where ΔV is potential difference between the spherical surfaces.

7. Synchrony

The condition to carry out the type of experiments described in this paper is necessary to achieve that the laser beam and molecular beam coincide both in time and space at the center of the electrode-meshes of TOF tube and that the detection and recorder system be ready to count the ions generated by the interaction between photons and molecules. To get synchrony, it was built a delay circuit using the chip SN74LS123 to control temporally the shot of the molecular beams [15]. The interaction between the two beam follows the next sequence: first the laser pulse produces a TTL which is introduced at the delay circuit and this generates a second TTL with a delay that can be changed according to the specific needs, in the present system this delayed TTL is used as the trigger to open the nozzle. The delay is about 98.7 ms and permits the first molecular pulse to interact with the second laser pulse and the cycle starts again. The nozzle is opened about $400 \mu s$ and pulse frequency is 10 Hz (the same of the laser). The TTL of the laser is used too to start the recorder in the multichannel scaler; therefore, each shot of the laser corresponds to a mass spectrum.

8. Recording and data processing

Recording and data processing is carried out using a multichannel scaler (EG&G ORTEC, Turbo-MCS). This instrument counts the event rate as a function of time. When accumulation starts, the MCS begins to count the input event (channeltron signal) in the first channel of its digital memory. At the end of the pre-selected dwell time the MCS advances to the next channel of memory to count the following events. This dwell and advance process is repeated until the MCS has scanned through all the channels in its memory. The display of the memory shows the counting rate of the input events versus time.

The most important features of the Turbo-MCS are: extremely wide range of operating parameters, with dwell time per channel selectable from of 5 ns to 65,535 seconds, and a scan length variable from 4 to 16,384 channels, time scans ranging from 20 ns to 10^9 seconds can be selected. It also accepts flexible input signals in the range of -5 V to $+5$ V, with a choice of discriminator triggering on either positive or negative slopes. The discriminator threshold is adjustable through the computer from -2.5 V to $+2.5$ V with 12-bit resolution. The MCS us connected to an IBM or IBM-compatible

personal computers through a cable and dual-port memory interface board that plugs into the computer and its software run under windows operating system [16].

In repetitive measurements, where the start of the scan can be synchronized with star of the event (laser pulse), multiple scan can be summed (our case) or averaged to diminish the statistical scattering in the recorded pattern. As it was pointed out, in this work we report results for multiphoton ionization and dissociation of acetone and multiphoton ionization of xenon, the mass spectrum were obtained summing 5,000 scans (5,000 laser shots). To record the mass spectra of the xenon, the dwell time used was 5 ns and 5,000 channels while for acetone the dwell time was 20 ns and 1,000 channels per scan. These parameters are chosen according the time of flight of the more massive ion, the sensibility of the detection and number of events.

9. Results

As it was mentioned above (Sec. 2), the experiment is started with a laser pulse, this pulse opens the pulsed valve and introduces the sample. If the sample is in liquid phase is mixed with He carrier gas.

Acetone seeded in He (1 atm) was expanded into the interaction chamber of the TOF, while xenon without carrier gas was expanded. Pulse duration of the pulsed valve was 400 μs . Mass spectra is obtained using the multichannel scaler and can be processing in its software or converted to ASCII format to process in any other software.

9.1. Calibration

The mass spectrometer was calibrated using (4+1) REMPI of the xenon at 499.050 nm. The xenon was chosen because its mass spectra is well known and presents a considerable number of isotopes. The mass spectra obtained is shown in Fig. 7. As it can be seen it is possible to resolve the peaks of the different isotopes for this atomic system.

Ionization of Xe at 499.050 nm is clearly a resonant multiphoton process in which the atom has to absorb four photons to reach the first excited state and one photon to be ionized (ionization potential is 12.078 eV) [17].

To calibrate the TOF spectrometer we selected, as reference, the Xe_{131}^+ isotope because offers a good resolution and intensity. From the Eq. (7) we obtained a relationship to calculate the time of flight of each different isotopes ionized. Because the kinetic energy is the same for all ions under the same experimental condition:

$$\frac{t_1}{\sqrt{m_1}} = \frac{t_2}{\sqrt{m_2}}. \quad (11)$$

If the isotope of reference reaches the detector in the time of flight $t_1 = 14.685 \mu\text{s}$ and its mass is $m_1 = 131 \text{ uma}$, from the Eq. (11) the peak centered at $t_2 = 14.704 \mu\text{s}$ corresponds to an ion of mass $m_2 = 132 \text{ uma}$, this mass coincide with the

isotope Xe_{132}^+ . By the same way it is possible to identify any ionic masses in the spectra.

In mass spectrometry it is conventional to measure the resolving power by the ratio $m/\Delta m$ where Δm is a discernable mass difference. In TOF mass spectrometry it is convenient to work in time domain. Thus the resolving power $m/\Delta m$ can be expressed in terms of $t/\Delta t$ as follows:

Since $m \propto t^2$, $m = At^2$ and $dm/dt = 2At$ where A is a constant; $dm/m = 2dt/t$ thus:

$$\frac{m}{\Delta m} = \frac{t}{2\Delta t}. \quad (12)$$

The finite time interval, Δt , corresponds to the full-width at half-maximum (height) of the peak (FWHM). Then the mass resolving power is limited by the difference in flight-time measured for ions of same mass.

To calculate the resolving power we use the peak centered at 14.545 μs corresponding to $m/z = 129$, in the mass spectra shown in Fig. 7. Figure 8 shows Lorentz fit of the peak $m/z = 129$, the resolution obtained is of ~ 460 which is an excellent figure for this type of instruments.

9.2. Multiphoton ionization and dissociation of acetone at 585 nm

The acetone is the molecule more studied because is the smallest of its type, and an additional motivation to this study is that the excited states involved in the multiphoton ionization correspond to resonant processes. Absorption studies have shown that the first band in acetone arises from the $S_1 \leftarrow S_0(p^* \leftarrow n)$ transition, which involves the promotion of a nonbonding electron on the oxygen atom to an antibonding electron on the carbonyl group. The absorption band, $S_1 0-0$, is located at 30435 cm^{-1} . Several theoretical studies suggest that a considerable number of valence states should exist in the 160-200 nm range, but no valence states with significant cross section in single-photon or two photon absorption have been found experimentally [18]. In addition the

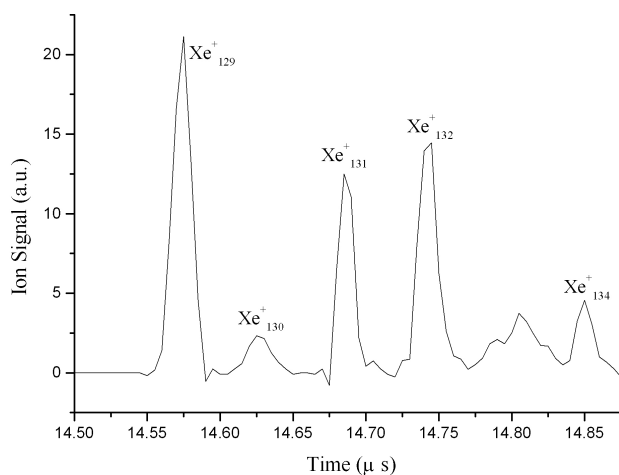
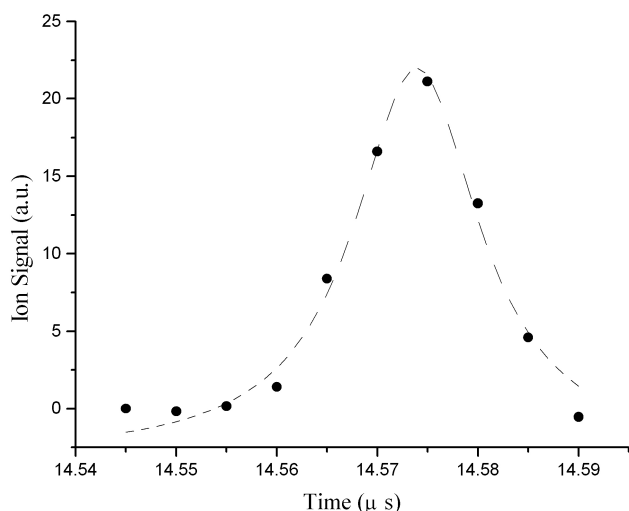


FIGURE 7. Multiphoton ionization time of flight mass spectrum of xenon at 499.050 nm.

FIGURE 8. Lorentz fit of the peak $m/z=129$.

acetone presents a set of Rydberg states. The $3s$ and $3p$ -Rydberg states are the most studied [19,20]. However, there are discrepancies between different wavelength experiments that involve different number of photons absorbed to reach the same state. One-photon experiments show that the $3s$ -Rydberg state is accessible with photons from 193 to 195 nm (6.42-6.35 eV). While two- and three-photon excitation studies have assigned the 0-0 band of the $3s$ -Rydberg state at 6.346 and 6.354 eV, respectively [20].

In the present investigation, the time of flight mass spectra of acetone at 585.000 nm were recorded; typical spectrum is shown in Fig. 9. The ionic fragment more abundant observed, in the mass spectra are: $m/e = 58, 43$ y 15 , corresponding to the molecular ion ($\text{CH}_3\text{COCH}_3^+$), acetyl ion (CH_3CO^+) and

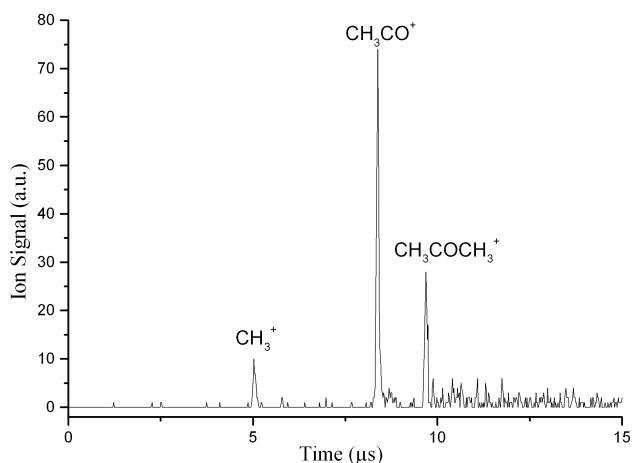
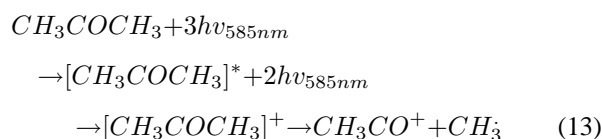


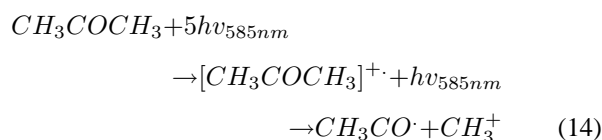
FIGURE 9. Multiphoton ionization time of flight mass spectra of acetone at 585.000 nm.

methyl ion (CH_3^+) respectively. There were also observed ionic fragments heavier than molecular acetone ions, these can be interpreted as an evidence of the cluster formation.

It has been demonstrated that multiphoton ionization of the acetone at 585 nm (~ 2.12 eV) is a resonant process ($3+2$) via $3s$ -Rydberg state. However, there are still controversies about the dissociation dynamics, particularly, about the breaking of the C-C bond to produce CH_3 y CH_3CO^* . S.A. Buzza *et al.* [18] have found that the acetone predissociates after excitation to the $3s$ -Rydberg state. In our experiment, the absorption of five photons at 585 nm delivers ~ 10.6 eV in the molecule. This energy is enough to dissociate the molecular ion in an acetyl ion and a methyl radical, because the ionization potential of acetone is 9.7 eV and the excess energy (0.9 eV) is sufficient to reach the threshold of dissociation and generate acetyl ion and methyl radical [21]:



The formation of methyl, CH_3^+ , ion requires the absorption of one additional photon by the molecular ion:



10. Conclusions

It was designed, set up, and operated a high-resolution multiphoton ionization and dissociation OPO based time of flight system. The mass spectrometer was calibrated using the resonant multiphoton time of flight mass spectra of xenon. The characteristic resolving power of the mass spectrometer is very good; 460 and allows to resolve the peaks corresponding to all mass of isotopes of the xenon. The multiphoton ionization and dissociation time of flight mass spectra of acetone at 585.000 nm and the peaks correspond to the molecular ion, the acetyl ion and the methyl ion were observed. The results agree with those obtained by S.A. Buzza, *et al.* [18] in femtosecond laser pulses regimen.

Acknowledgment

The authors wish to thank CONACYT, DGAP, and CLAF-M by financial support. The authors thank A. Guerrero and A. Bustos for technical support.

1. K.W.D. Ledingham and R.P. Singhal, *Int. J. Mass Spectrom. Ion Processes*. **163** (1997) 149.
2. U. Boesl, *J. Mass Spectrom.* **35** (2000) 289.
3. A. Aguilar, *Identificación de niveles excitados del xenon por ionización multifotónica resonante en un tubo de tiempo de vuelo*, Facultad de Ciencias, UNAM, México, DF. 1997. Tesis de licenciatura.
4. Pulsed Nd:YAG Laser, Quanta Ray, Series PRO-210, User's Manual. Spectra-Physics, Inc. Mountain View (1998).
5. G.S. He and S.H. Liu, *Physics of Nonlinear Optics* (World Scientific Publishing Co. Singapore, 1999).
6. Optical Parametric Oscillator, MOPO-730, User's Manual, Quanta Ray, Spectra-Physics Inc. Mountain View 1995.
7. A. Kantrowitz and J. Grey, *Rev. of Sci. Instrum.* **22** (1953) 328.
8. A. Kantrowitz and J. Grey, *Rev. of Sci. Instrum.* **22** (1953) 333.
9. R.E. Smalley, L. Wharton, and D.H. Levy, *Spectrosc. with Supersonic Jets*. **10** (1977) 139.
10. B.a. Mamyrin, *Int. J. of Mass Spectrom.* **206** (2001) 251.
11. M. Guilhaus, D. Selby, and V. Mlynski, *Mass Spectrom. Rev.* **19** (2000) 65.
12. M. Guilhaus, *J. Mass Spectrom.* **30** (1995) 1519È.
13. W.C. Wiley and I.H. McLaren, *Rev. Sci. Instrum.* **26** (1955) 1150.
14. *Electrostatic Energy Analyzer, AC-900B*, User's Manual, COMSTOCK Inc. Oak Ridge, TN. 1998.
15. J.P. Flores, *Procesos multifotónicos en el monóxido de carbono*, Facultad de Ciencias, UNAM. México, 2001. Tesis de licenciatura.
16. *Turbo-MCS A67-BI*, User's Manual, EG&E ORTEC, USA.
17. P. Hansch, M.A. Walker, and L.D. Van Woerkom, *Phys. Rev. A.* **54** (1996) R2559.
18. S.A. Buzza, E.M. Zinder, and A.W. Castleman, Jr. *J. Chem. Phys.* **104** (1996) 5040.
19. Q. Zhong, L. Poth, and A.W. Castleman, Jr. *J. Chem. Phys.* **110** (1999) 195.
20. J.G. Philis and L. Goodman, *J. Chem. Phys.* **98** (1993) 3795.
21. C. Majumder, *et al.*, *Chem. Phys. Lett.* **304** (1999) 51.